

Intersystem crossing in the exit channel

Hongwei Li¹⁰, Alexander Kamasah¹, Spiridoula Matsika² and Arthur G. Suits¹*

Intersystem crossing plays an important role in photochemistry. It is understood to be efficient when heavy atoms are present due to strong spin-orbit coupling, or when strongly bound long-lived complexes are formed that increase the chance of finding the singlet-triplet intersection seam. Here we present evidence for a different intersystem crossing mechanism in the bimolecular reaction of O(³P) with alkylamines. In crossed-beam experiments, product velocity-flux maps are measured for aminoalkyl radicals produced from H abstraction from the methyl group, which also gives OH radicals as co-fragments. The low translational-energy release and isotropic angular distributions of the products indicate that such reactions undergo the formation of a complex before OH and aminoalkyl are produced. However, there is no well on the triplet potential energy surface that could support such a complex. Multi-reference ab initio calculations suggest, instead, that intersystem crossing occurs in the exit-channel region due to the long-range dipole-dipole interaction between the nascent radical product pair coupled with the vanishing singlet-triplet splitting at long range. Intersystem crossing then leads to a deep hydroxylamine well before OH elimination.

ntersystem crossing (ISC), the non-radiative transition between two electronic states with different spin multiplicity, is ubiquitous and important in fields ranging from chemical physics to chemical biology. ISC is involved in a wide range of applications including materials science¹, molecular photonics², photosensitizers³ and photodynamic therapy for cancer⁴. It is well known that the 'heavy atom effect' promotes ISC, because the inclusion of heavy atoms in the molecular structure enhances the spin-orbit coupling between singlet and triplet states^{5,6}. ISC is also observed in oxygen atom reactions with unsaturated hydrocarbons, in which case the strongly bound addition complex is long-lived, increasing the probability for the system to access the singlet-triplet seam of intersection where ISC occurs⁷⁻¹². Here, we show that, even in the absence of heavy atoms or a strongly bound adduct on the initial triplet potential surface, ISC occurs in the course of bimolecular reactions of O(3P) with amines. In this case, we propose that ISC is promoted by the near degeneracy of the singlet and triplet potential surfaces in the exit channel, along with the long-range dipole-dipole interaction and high dimensionality of the system that permits a brief period of recollision, leading finally to the deep hydroxylamine well on the

Here, we investigate the mechanism of the elementary reactions in the initial combustion process, reaction of the O(³P) radical with amines, dimethylamine (DMA) and trimethylamine (TMA). We characterized the translational-energy release and angular distributions during the reactions using crossed-beam scattering combined with universal d.c. slice imaging, as described previously¹³. Highlevel ab initio calculations on the energies, structures and spin–orbit coupling along the reaction pathways were also performed to gain insight into the underlying dynamics. Combining these experimental and theoretical studies suggests that ISC from triplet to singlet potential energy surfaces (PESs) in the exit channel plays an important role in the bimolecular reaction dynamics for O(³P) reaction with amines.

Results

The electronic ground-state atomic oxygen, $O(^{3}P)$, was generated from the photolysis of SO_{2} using 193 nm radiation. Amines (DMA

or TMA) seeded in helium were crossed with the O(3 P) beam at 90° under single-collision conditions. The scattered products from the bimolecular reaction were ionized at the interaction region by an F_2 excimer laser (157 nm, 7.9 eV). The ions were then accelerated onto a position-sensitive detector gated to select a specific m/z ratio. The resultant ion images were recorded with a charge-coupled device camera, using a high-resolution real-time ion counting method using our megapixel acquisition program NuACQ 14 . The sliced and centroided images were accumulated, reflecting the product velocity–flux contour maps with the speed and angular information for the reaction.

For the bimolecular reaction of O(3P) with DMA at a collision energy of $E_{coll} = 7.8 \,\mathrm{kcal} \,\mathrm{mol}^{-1}$ we detected only one product channel, m/z 44, under our experimental conditions. This indicates an H abstraction pathway producing the C2H6N radical with a hydroxyl radical (OH) co-fragment. There are two isomers for the C2H6N radical: CH₃NHCH₂ (arising from H abstraction at the methyl site) and N(CH₃)₂ (produced by abstraction at the nitrogen). Ab initio calculations performed using the CBS-QB3 method¹⁵ implemented in the Gaussian09 quantum chemistry software package¹⁶ were used to determine ionization energies for these product radicals. The calculations predict that the CH₃NHCH₂ radical has a vertical ionization energy of 6.7 eV, easily accessed with our detection limit of 7.9 eV, whereas the N(CH₃), radical has a much higher vertical ionization energy of 9.5 eV. Therefore, only the CH₃NHCH₂ radical product is detected under our experimental conditions, even though the N(CH₃)₂ radical is also a possible product from this reaction. This was also proved by checking the reaction of O(3P) with the partially deuterated isotopologue (CD₃)₂NH (Supplementary Experimental Results). Only the CD₃NHCD₂ radical product was observed by our 7.9 eV probe, consistent with the ionization energy calculations. This indicates that the H/D removal by the O(3P) radical we detected occurs at the methyl site rather than the amine site.

The corresponding product scattering image after background subtraction and density-to-flux correction is shown in Fig. 1, with a Newton diagram superimposed. The scattered radical products are examined in three distinct centre-of-mass (c.o.m.) angular ranges defined with respect to the DMA beam direction: forward

ARTICLES NATURE CHEMISTRY

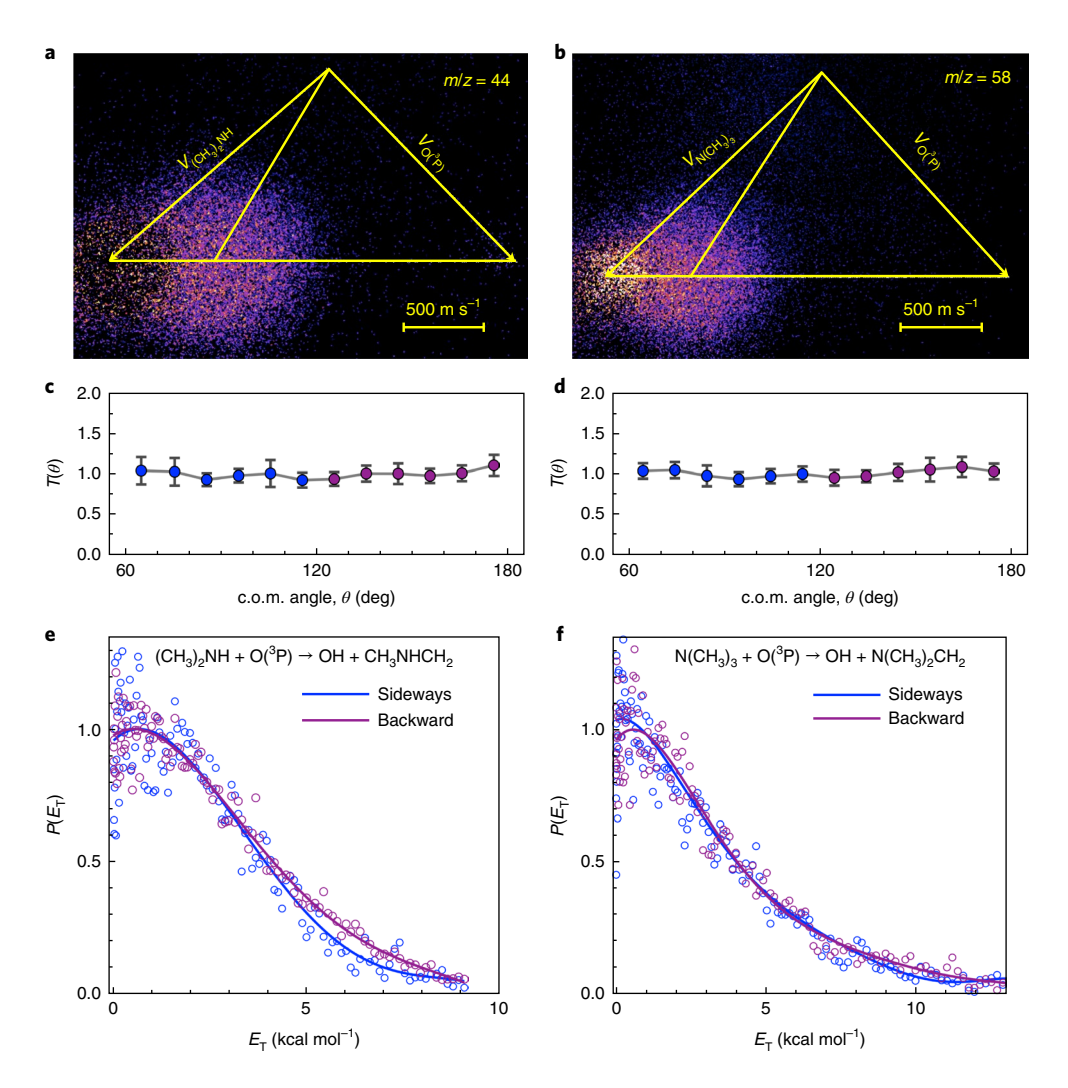


Fig. 1 | **Velocity-flux contour map analysis of aminoalkyl products from reactions of O(³P) with DMA and TMA. a-f**, Shown are d.c. slice images (**a,b**) with Newton diagrams superimposed, and c.o.m. angular $T(\theta)$ (**c,d**) and translational-energy $P(E_T)$ (**e,f**) distributions for the reactions of O(³P) with DMA (**a,c,e**) and TMA (**b,d,f**) at collision energies of 8.0 and 7.8 kcal mol⁻¹, respectively. The SW (60-120°) component is in blue and the BW component in purple (120-180°). The $P(E_T)$ curves are fitted by least-squares polynomial regressions to guide the eye. $T(\theta)$ values are shown averaged every 10°, with error bars ($\pm \sigma$) estimated by mean absolute deviation of the raw data in the corresponding angle range. The isotropic angular distributions and low translational-energy release of the products indicate that such reactions undergo the formation of a complex before OH and aminoalkyl are produced.

(FW, 0-60°), sideways (SW, 60-120°) and backward (BW, 120-180°). Although the FW component is obscured by a strong photochemical background, the SW and BW components clearly reveal the underlying dynamics. The c.o.m. translational-energy release distributions $P(E_T)$ of both SW and BW components peak at low energy, ~10% of the collision energy (Fig. 1e). The c.o.m. angular distribution $T(\theta)$ (Fig. 1c), including both SW and BW contributions, is flat, consistent with the isotropic image observed. These experimental results clearly indicate an indirect reaction mechanism. Formation of a long-lived adduct in a bimolecular reaction results in product translational-energy distributions that peak at low energy because of randomization of the internal energy over the vibrational degrees of freedom in the complex. Additionally, if the complex lifetime is much longer than its rotational period, the system loses reference to the initial approach direction, giving rise to a symmetric scattering in the FW and BW directions and identical translational-energy distributions in all directions. For complicated polyatomic systems in which the scattering is non-planar, this symmetric scattering becomes fully isotropic¹⁷. Therefore, the low translational-energy release and isotropic angular distributions of the scattered products

indicate the importance of the complex-elimination mechanism in a bimolecular reaction of the O(³P) atom with DMA.

Similar low translational-energy release and isotropic angular distributions were also obtained here for the O(³P) reactions with TMA (Fig. 1d-f) and partially deuterated DMA, (CD₃)₂NH (Supplementary Experimental Results), confirming again that the complex-elimination mechanism plays an important role in bimolecular reactions of O(³P) with amines to produce OH and aminoalkyl radicals. The complex-elimination mechanism observed here agrees well with the previous cross-jet reactor study and kinetic measurements performed decades ago for the title reactions^{18,19}.

The crucial underlying question now is the pathway for OH elimination from the complex. A careful search along the triplet and singlet PESs was performed by ab initio calculations at the CBS-QB3 level of theory. For the triplet PESs of the O(³P)+DMA reaction, as shown in Fig. 2, we could not locate any transition state for the direct H abstraction pathway to generate the OH and CH₃NHCH₂ products that we probed experimentally. This suggests that the direct reaction is barrierless. Interestingly, we find a roaming-type transition state (TS-Roam) that has one low

NATURE CHEMISTRY ARTICLES

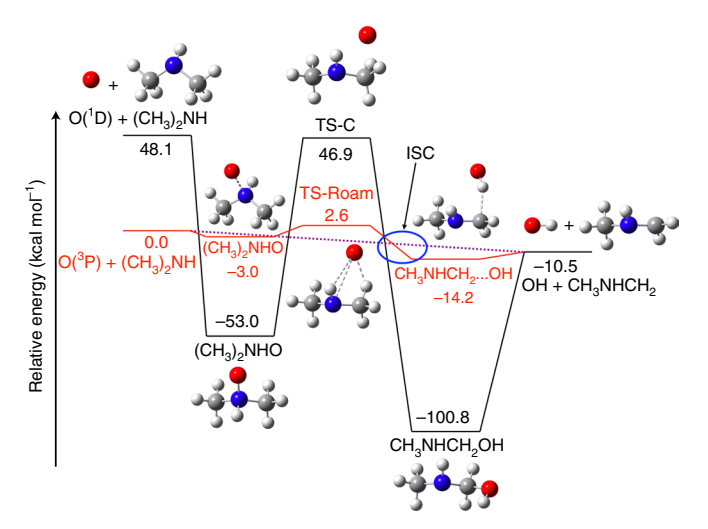


Fig. 2 | Key points on the triplet and singlet PESs of the O(³P) + DMA reaction. The red solid line illustrates the roaming pathway on the triplet PES and the black solid line shows the pathway on the singlet PES with two deep wells in the entrance and exit channel regions. The purple dashed line illustrates the barrierless direct H abstraction pathway on the triplet surface with ISC occurrence schematically indicated by a blue oval. All calculations were performed at the CBS-QB3 level of theory with relative energies shown in kcal mol⁻¹.

imaginary frequency (190 cm⁻¹), indicating a flat PES in this region, and two very low bound frequencies (120 and 180 cm⁻¹) corresponding to motions of the O atom relative to the DMA fragment. This roaming-type transition state connects two shallow van der Waals complex wells, (CH₃)₂NHO and CH₃NHCH₂···OH, in the reaction pathway. However, based on the observed long-lived complex formation and relatively high collision energy $E_{coll} = 7.8 \, \text{kcal mol}^{-1}$ in the experiment, this shallow well is not likely to be a key aspect of the reaction. We then searched through the singlet PESs because the coupling between singlet and triplet PESs inducing ISC is ubiquitous in chemistry and is widely observed in O(3P) reactions with unsaturated hydrocarbons such as C₂H₄ and CH₂CCH₂ (refs ^{8,10,20}). As shown in the singlet PESs for the $O(^{3}P) + DMA$ reaction in Fig. 2, one transition state (TS-C) and two very deep complex wells ((CH₃)₂NHO and CH₃NHCH₂OH) are located on the reaction pathway to form the probed products. However, the TS-C found here is followed by a very high barrier energy, 46.9 kcal mol⁻¹ above the O(³P) + DMA reactant asymptotic limit. Given the experimental collision energy of 7.8 kcal mol⁻¹, the system does not have enough energy to surmount this barrier to form the detected products if the reaction accesses the singlet (CH₃)₂NHO entrance complex well via ISC. Therefore, the only plausible pathway for the reaction will be that the O(3P) radical attacks DMA to initiate direct H abstraction from methyl group. Then, due to the long-range dipole-dipole interaction and the high dimensionality of the system, OH and CH₃NHCH₂ radicals do not part immediately but undergo multiple collisions. At the region where both triplet and singlet PESs have similar energy (indicated by the blue oval in Fig. 2), the system hops from triplet to singlet surface and then falls into a very deep hydroxylamine well, forming CH₃NHCH₂OH 100 kcal mol⁻¹ lower in energy than the reactants. The system will stay in the CH₃NHCH₂OH well for a time much longer than the rotational period of the complex, then eliminates the OH radical. In this case, the reaction mechanism features ISC leading to long-lived complex formation rather than being caused by it. The analogous PESs for the O(3P) + TMA reaction were also calculated at same level of theory as shown

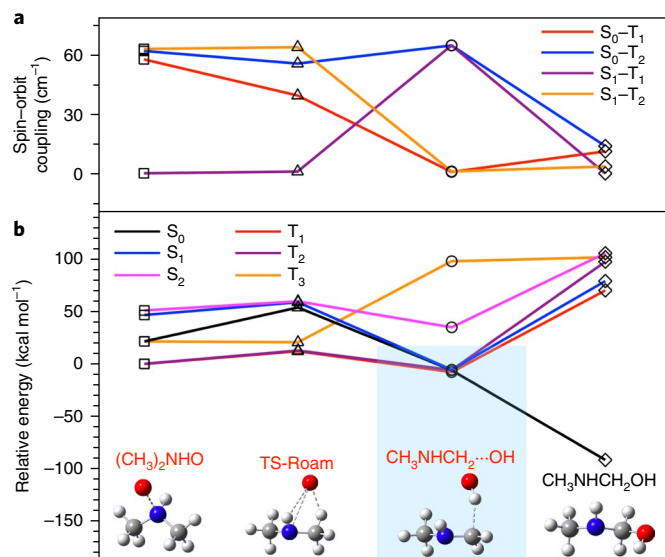


Fig. 3 | Spin-orbit coupling and high level energy calculations.

a, Spin-orbit coupling (calculated at the CASSCF(4,4)/cc-pvdz level of theory) along the optimized important points on the pathway of the O(3 P) + DMA reaction. The geometric structures of (CH $_3$) $_2$ NHO, TS-Roam and CH $_3$ NHCH $_2$ ···OH are optimized on the triplet surface and the CH $_3$ NHCH $_2$ OH structure is optimized on the singlet surface. **b**, Energies (calculated at the MCQDPT2(6,6)/cc-pvdz level of theory) of the first three singlet (S $_0$, S $_1$ and S $_2$) and three triplet (T $_1$, T $_2$ and T $_3$) states at the same optimized points. All six state energies are relative to the lowest energy of the triplet (CH $_3$) $_2$ NHO entrance complex. The PESs are nearly degenerate in the exit channel, as indicated by the blue shaded area. Grey, carbon; blue, nitrogen; red, oxygen;

white, hydrogen.

in the Supplementary Calculation Results, indicating the same reaction mechanism.

Further effort has been devoted to characterizing the energies of the first six states (three singlets and three triplets) at the optimized important points ((CH₃)₂NHO, TS-Roam, CH₃NHCH₂···OH on the triplet surface and CH₃NHCH₂OH on the singlet surface) along the reaction pathway of the $O(^{3}P) + DMA$ reaction (Fig. 3). These energy calculations were performed in the GAMESS suite of programs^{21,22} using the multi-configuration quasi-degenerate perturbation theory (MCQDPT2) method^{23,24} including dynamical and non-dynamical correlation with the cc-pvdz basis. The orbitals were obtained from a six-state averaged complete active space self-consistent field (CASSCF) method with an active space of six electrons in six orbitals (6,6). Figure 3b shows that the first two triplet states (T_1 and T_2) in the entrance channel complex are almost degenerate and about 0.9 eV below the first singlet state. At the transition state region, the energy gap between the triplet and singlet states is even larger, close to 2 eV, due to the localization on the O atom (whose singlet-triplet splitting is ~2 eV.) However, in the exit channel complex region, the energies of the first two singlet and two triplet states are very close (ranging from 0.3 to 2.3 kcal mol⁻¹), giving rise to degenerate surfaces. In addition, the spin-orbit couplings between these singlet and triplet states were calculated at the CASSCF(4,4)/cc-pvdz level of theory. Figure 3a shows that the spin-orbit couplings between two pairs of singlet-triplet states are close to 60 cm⁻¹ for the exit channel complex on the triplet surface and drop to 10 cm⁻¹ or less for the CH3NHCH2OH deep well on the singlet surface. The strength of the spin-orbit coupling can be understood by the nature of the wavefunction at each geometry and the El Sayed rules²⁵. At the ARTICLES NATURE CHEMISTRY

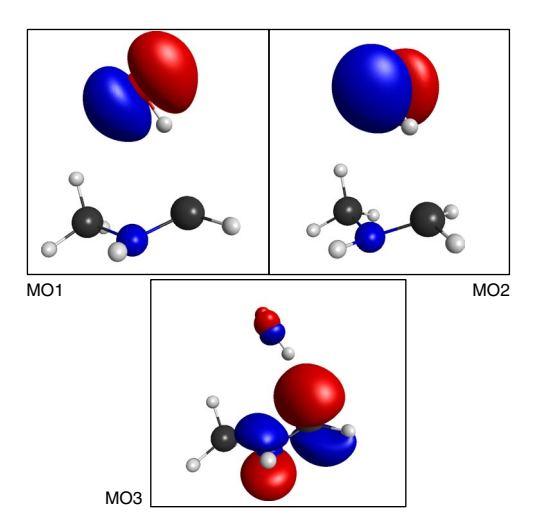


Fig. 4 | Orbitals participating in the wavefunctions of S₀, **S**₁, **T**₁ and **T**₂. The orbitals are taken from the CASSCF(4,4) calculation at the $CH_3NHCH_2...OH$ geometry illustrated by the lobes with different phases (shown in red and blue). Black, carbon; blue, nitrogen; red, oxygen; white, hydrogen.

triplet CH₃NHCH₂···OH van der Waals complex minimum, the configurations describing the two singlet and two triplet states are:

 $\Psi(S_0)$: (MO1)²(MO2)¹(MO3)¹ $\Psi(S_1)$: (MO1)¹(MO2)²(MO3)¹ $\Psi(T_1)$: (MO1)²(MO2)¹(MO3)¹ $\Psi(T_2)$: (MO1)¹(MO2)²(MO3)¹

where the two unpaired electrons are combined with a singlet spin wavefunction while in the triplet states they are combined with a triplet spin wavefunction. The corresponding orbitals are shown in Fig. 4. According to the El Sayed rules, singlet–triplet spin–orbit coupling is stronger when the orbital angular momentum changes as the spin changes. The character of the wavefunctions shows that S_0 and T_1 (similarly for S_1 and T_2) have the same configuration so there is no angular momentum change in this case and the corresponding spin–orbit coupling is small (Fig. 3a). However, only one electron is required to change from the S_0 to T_2 configuration (similarly from S_1 to T_1), and it is accompanied by a change in angular momentum but only a small change in electronic density (Fig. 4). As a result, the corresponding spin–orbit coupling is large for the S_0 – T_2 and S_1 – T_1 pairs.

Discussion

We have shown that the spin-orbit coupling is large and the surfaces are degenerate for the 'OH-CH3NHCH2' radical pair. It remains for us to demonstrate that the initial abstraction dynamics can give rise to extended interaction between these radicals. To this end we performed direct dynamics classical trajectory calculations of the H abstraction process on the triplet surface performed using a Born-Oppenheimer molecular dynamics (BOMD) model at the B3LYP/6-31G(d) level of theory. Significant insight regarding the reaction dynamics is gained by looking at representative trajectories. Snapshots of one typical trajectory are illustrated in Fig. 5, and its full animation is provided in the Supplementary Movie. This trajectory was started from a transition state (located at the B3LYP/6-31G(d) level of theory, but disappears at higher levels) for the direct H abstraction process with 8 kcal mol⁻¹ initial kinetic energy in the reaction coordinate. As shown in Fig. 5, the H atom is quickly transferred from the methyl group to the O atom at

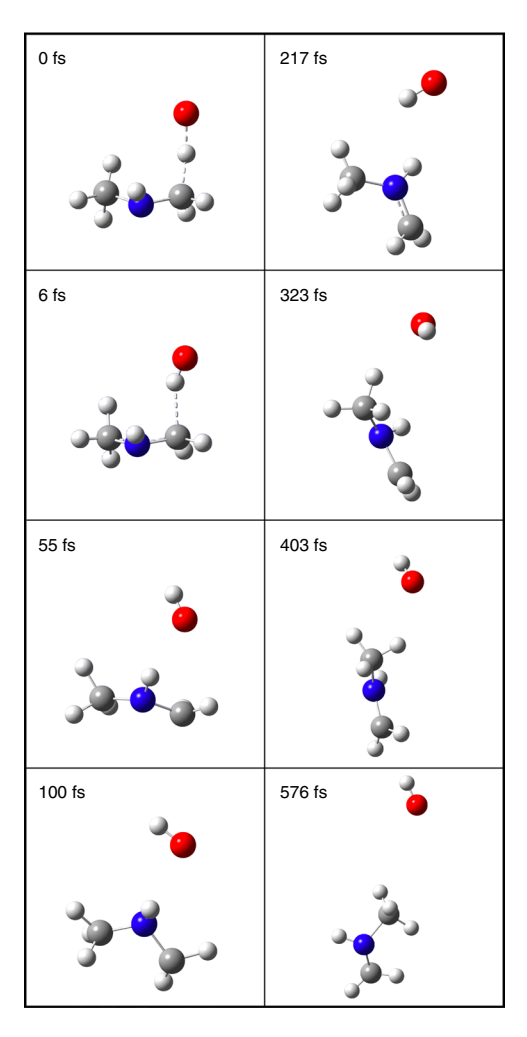


Fig. 5 | Snapshots of a representative trajectory. The trajectory starts from the transition state of the direct H abstraction process to $OH + CH_3NHCH_2$ products on the triplet surface. The H atom is quickly transferred to the O atom (6 fs) to form OH and CH_3NHCH_2 radicals. The OH radical does not leave immediately but roams around the CH_3NHCH_2 radical for about half a picosecond before dissociation. Grey, carbon; blue, nitrogen; red, oxygen; white, hydrogen. An animation of the full trajectory is available as a Supplementary Movie.

6fs to produce 'OH and CH3NHCH3' radicals. Instead of parting immediately, the 'OH radical roams around the CH3NHCH2' radical for about half a picosecond before elimination. This lifetime is too short to account for the isotropic distribution observed experimentally, but it is accompanied by a period of recollision, which is not unusual for a system of this nature. In addition, due to the degenerate singlet and triplet potential surfaces and relatively strong spin-orbit coupling in the exit channel region, the intersection seam of the singlet and triplet surfaces will be crossed many times, which permits very efficient ISC and access to the very deep well on the singlet surface. Although direct abstraction is possible on the triplet surface, the absence of a direct component in the experiment (which would be seen as backward scattering and a translational-energy distribution peaking away from zero) indicates that this reaction-mediated ISC is very efficient in this case, accounting for at least 90% of the flux. ISC must be fast here (a few hundred femtoseconds timescale) to be able to compete with the direct abstraction process. This fast ISC is attributed to the degeneracy of the singlet and triplet states, the relatively strong spin-orbit coupling, and the dynamics of the interacting radical pair. Ultrafast NATURE CHEMISTRY ARTICLES

ISC in the photoexcitation of 2-nitronaphthalene has recently been measured experimentally as 700 fs, which also requires the angular momentum of only one electron to change and small geometrical arrangements to approach the ISC configurations²⁶. The fact that the singlet surface of the $O(^3P)+DMA$ reaction is much steeper in the exit channel probably helps to remove the population very quickly after ISC. Once the system undergoes ISC it will rapidly move away on the singlet surface toward the minimum, while the triplet surface is very flat and there is no strong driving force for moving away.

ISC in O(3P) reactions with unsaturated hydrocarbons has been well documented, and provides a clear contrast to what is seen here⁷. The trajectory surface hopping calculations from Bowman and coworkers clearly reveal the mechanism in that case^{8,20}. For $O(^{3}P)$ + ethylene, there is a diradical addition complex bound by 25 kcal mol⁻¹ that supports a long-lived complex. The bound diradical system hops to the nearby singlet potential surface where that configuration is a transition state connecting oxirane and acetaldehyde. The energy gap between the triplet and singlet surfaces is ~1,150 cm⁻¹ on average, and the spin-orbit coupling is 35 cm⁻¹ at the hopping configurations. Once on the singlet surface, a number of product channels are open to it. A key feature these two mechanisms have in common is the presence of two radical sites that are weakly coupled: for O(3P)+ethylene it is within the OCH2CH2 diradical, while for O(3P)+DMA it is the two radicals OH and CH₃NHCH₂ interacting in the exit channel.

In conclusion, we have investigated the dynamics of the H abstraction process from the methyl group of amines (DMA and TMA) when reacting with ground state O(³P). Characterization of the low product translational-energy release and isotropic angular distributions indicates that such reactions undergo complex formation first, before producing OH and aminoalkyl products. Ab initio calculations indicate that the reaction is initiated by direct H abstraction from O attack, and then proceeds via efficient ISC to the singlet surface, forming a long-lived complex before OH elimination. This fast ISC occurs in the exit channel as a result of interactions between the incipient radical pair. This mechanism is not exclusive to amine reactions, and similar dynamics may occur in a large range of related systems yet to be studied.

Methods

Crossed-beam slice imaging experiment. The experiments were conducted on a crossed-beam scattering apparatus combined with universal d.c. slice imaging as described previously 13,27,28. Briefly, the apparatus consists of one reaction chamber and two source chambers that are perpendicular to each other. 5% SO₂ seeded in He at a backing pressure of 60 p.s.i.g. was pulsed into one source chamber via a piezoelectric stack actuator valve29 into a quartz capillary tube (1 mm inner diameter; 10 mm length). The electronic ground state O(3P) beam was generated from the photolysis of SO₂ by the 193 nm output of an ArF excimer laser (GamLaser, Ex200), which was loosely focused along the length of the capillary tube using a cylindrical lens. The photolysis of SO₂ in this way does not generate any electronic excited oxygen $O(^1\mathrm{D})$, but only ground state oxygen $O(^3P)^{30,31}$. The population distribution of the $O(^3P_{J=2,1,0})$ fine structure from the source was measured to be ~10:3:1 for J = 2, 1, 0 assuming equal total two-photon absorption cross-sections. Amines, dimethylamine (DMA) or trimethylamine (TMA) were seeded in He (5%) and introduced into the second source chamber by a piezoelectric pulsed valve with a backing pressure of 60 p.s.i.g. Both molecular beams were collimated by a 1-mm-diameter skimmer before entering the reaction chamber, and intersected with each other at an angle of 90°. The scattered radical products were ionized with vacuum ultraviolet 157 nm radiation (7.9 eV) from a F₂ excimer laser (GamLaser, Ex10). Ions were initially accelerated by a four-electrode d.c. slice ion optics assembly, and velocity-focused onto a dual microchannel plate/phosphor screen coupled detector after passing through a 75 cm field-free flight tube. The detector was gated for the centre slice of the scattered product ions at a specific m/z ratio. Ion images were recorded using a charge-coupled device camera, employed with a high-resolution real-time ion counting method by our megapixel acquisition program NuACQ14. The data presented in the main text are shown after background subtraction and densityto-flux corrections. Background images were taken with the 193 nm photolysis laser off and induced from the photodissociation of amines by the probe laser.

Density-to-flux correction was performed by scaling the pixel intensity by the lab velocity at each point on the image.

Computational methods. Ab initio calculations (including geometric structure and energy, and ionization energy calculation) were performed using the CBS-QB3 method¹⁵, B3LYP/6-311G(2d,d,p) and wB97XD/6-311+G(2d,p) or wB97XD/ 6-311G(2d,d,p), implemented in the Gaussian09 quantum chemistry software package¹⁶. Connections between the transition state and local minima were verified by intrinsic reaction coordinate calculations at the B3LYP/6-311+G(2d,p) and B3LYP/6-311G(2d,d,p) level of theory. A direct dynamics classical trajectory calculation of the H abstraction process on the triplet surface was performed using a BOMD model at the B3LYP/6-31G(d) level of theory. This trajectory was started from a transition state (located at the B3LYP/6-31G(d) level of theory, but which disappears at higher levels) of the direct H abstraction pathway with 8 kcal molinitial kinetic energy in the reaction coordinate. The whole trajectory was run with a time up to 1.2 ps. Further efforts were devoted to determining the energies of the first six states (three singlets and three triplets), and spin-orbit couplings were calculated for the O(3P) + DMA system. The quasi-degenerate perturbation theory (MCQDPT2) method^{23,24}, which includes both dynamical and non-dynamical correlation, was used to calculate the energies of the first six states at the optimized important points ((CH₃)₂NHO, TS-Roam, CH₃NHCH₂···OH on the triplet surface and CH3NHCH2OH on the singlet surface) along the O(3P) + DMA reaction pathway. The orbitals were obtained from a six-state averaged CASSCF with an active space of six electrons in six orbitals. Dynamical correlation is very important for the energies in this case. However, the spin-orbit coupling is expected to be relatively insensitive to dynamical correlation. Furthermore, the spin-orbit coupling implementation is only available at the CASSCF level in the GAMESS suite of programs. Two different active spaces, (6,6) and (4,4), were used, and both gave very similar results. The cc-pvdz basis set was used in all calculations, as well as the GAMESS suite of programs^{21,22}.

Data availability

The authors confirm that all relevant data are included in the paper and/or its Supplementary Information, except raw image data, which are available on reasonable request from the authors.

Received: 9 February 2018; Accepted: 6 November 2018; Published online: 10 December 2018

References

- Bolton, O., Lee, K., Kim, H. J., Lin, K. Y. & Kim, J. Activating efficient phosphorescence from purely organic materials by crystal design. *Nat. Chem.* 3, 205–210 (2011).
- Goushi, K., Yoshida, K., Sato, K. & Adachi, C. Organic light-emitting diodes employing efficient reverse intersystem crossing for triplet-to-singlet state conversion. *Nat. Photon.* 6, 253–258 (2012).
- Zhao, J. Z., Wu, W. H., Sun, J. F. & Guo, S. Triplet photosensitizers: from molecular design to applications. *Chem. Soc. Rev.* 42, 5323–5351 (2013).
- Kamkaew, A. et al. BODIPY dyes in photodynamic therapy. Chem. Soc. Rev. 42, 77–88 (2013).
- Koziar, J. C. & Cowan, D. O. Photochemical heavy-atom effects. Acc. Chem. Res. 11, 334–341 (1978).
- Alagia, M. et al. Crossed beam studies of the O(³P,¹D) + CH₃I reactions: direct evidence of intersystem crossing. Faraday Discuss. 113, 133–150 (1999).
- Casavecchia, P., Leonori, F. & Balucani, N. Reaction dynamics of oxygen atoms with unsaturated hydrocarbons from crossed molecular beam studies: primary products, branching ratios and role of intersystem crossing. *Int. Rev. Phys. Chem.* 34, 161–204 (2015).
- Fu, B. N. et al. Intersystem crossing and dynamics in O(³P) + C₂H₄ multichannel reaction: experiment validates theory. *Proc. Natl Acad. Sci. USA* 109, 9733–9738 (2012).
- Leonori, F. et al. Experimental and theoretical studies on the dynamics of the O(³P)+propene reaction: primary products, branching ratios and role of intersystem crossing. *J. Phys. Chem. C* 119, 14632–14652 (2015).
- Leonori, F. et al. Crossed molecular beam dynamics studies of the O(³P)+allene reaction: primary products, branching ratios and dominant role of intersystem crossing. *J. Phys. Chem. Lett.* 3, 75–80 (2012).
- Schmoltner, A. M., Chu, P. M., Brudzynski, R. J. & Lee, Y. T. Crossed molecular beam study of the reaction O(³P) + C₂H₄. J. Chem. Phys. 91, 6926–6936 (1989).
- Schmoltner, A. M., Huang, S. Y., Brudzynski, R. J., Chu, P. M. & Lee, Y. T. Crossed molecular-beam study of the reaction O(³P) + allene. *J. Chem. Phys.* 99, 1644–1653 (1993).
- Joalland, B. et al. Dynamics of chlorine atom reactions with hydrocarbons: insights from imaging the radical product in crossed beams. *J. Phys. Chem. A* 118, 9281–9295 (2014).
- Li, W., Chambreau, S. D., Lahanker, S. A. & Suits, A. G. Megapixel ion imaging with standard video. *Rev. Sci. Instrum.* 76, 063106 (2005).

ARTICLES NATURE CHEMISTRY

- Montgomery, J. A., Frisch, M. J., Ochterski, J. W. & Petersson, G. A. A complete basis set model chemistry. VII. Use of the minimum population localization method. J. Chem. Phys. 112, 6532–6542 (2000).
- 16. Frisch, M. J. et al. Gaussian 09 Revision D.01 (Gaussian, 2013).
- Joalland, B., Shi, Y., Kamasah, A., Suits, A. G. & Mebel, A. M. Roaming dynamics in radical addition-elimination reactions. *Nat. Commun.* 5, 4064 (2014).
- Slagle, I. R., Dudich, J. F. & Gutman, D. Identification of reactive routes in the reactions of oxygen atoms with methylamine, dimethylamine, trimethylamine, ethylamine, diethylamine and triethylamine. J. Phys. Chem. 83, 3065–3070 (1979).
- Atkinson, R. & Pitts, J. N. Kinetics of the reactions of O(³P) atoms with the amines CH₃NH₂, C₂H₅NH₂, (CH₃)₂NH, and (CH₃)₃N over the temperature range 298–440 °K. J. Chem. Phys. 68, 911–915 (1978).
- Balucani, N., Leonori, F., Casavecchia, P., Fu, B. N. & Bowman, J. M. Crossed molecular beams and quasiclassical trajectory surface hopping studies of the multichannel nonadiabatic O(³P)+ethylene reaction at high collision energy. *J. Phys. Chem. A* 119, 12498–12511 (2015).
- Schmidt, M. W. et al. General atomic and molecular electronic structure system. J. Comput. Chem. 14, 1347–1363 (1993).
- Gordon, M. S. & Schmidt, M. W. in Theory and Applications of Computational Chemistry: The First Forty Years (eds Dykstra, D. E., Frenking, K. S. K. & Scuseria, G. E.) 1167–1189 (Elsevier, Amsterdam, 2005).
- Nakano, H. Quasidegenerate perturbation theory with multiconfigurational self-consistent-field reference functions. J. Chem. Phys. 99, 7983–7992 (1993).
- Nakano, H. MCSCF reference quasidegenerate perturbation theory with Epstein–Nesbet partitioning. Chem. Phys. Lett. 207, 372–378 (1993).
- 25. El-Sayed, M. A. Spin-orbit coupling and the radiationless processes in nitrogen heterocyclics. *I. Chem. Phys.* **38**, 2834–2838 (1963).
- Zobel, J. P., Nogueira, J. J. & González, L. Mechanism of ultrafast intersystem crossing in 2-nitronaphthalene. Chem. Eur. J. 24, 5379–5387 (2018).
- Ahmed, M., Peterka, D. S. & Suits, A. G. Imaging H abstraction dynamics in crossed molecular beams: Cl+ROH reactions. *Phys. Chem. Chem. Phys.* 2, 861–868 (2000).
- 28. Huang, C., Li, W. & Suits, A. G. Rotationally resolved reactive scattering: imaging detailed $Cl+C_2H_6$ reaction dynamics. *J. Chem. Phys.* **125**, 133107 (2006).

- Abeysekera, C. et al. Note: a short-pulse high-intensity molecular beam valve based on a piezoelectric stack actuator. Rev. Sci. Instrum. 85, 116107 (2014).
- Kawasaki, M. & Sato, H. Photodissociation of molecular beams of SO₂ at 193 nm. Chem. Phys. Lett. 139, 585–588 (1987).
- 31. Felder, P., Effenhauser, C. S., Haas, B. M. & Huber, J. R. Photodissociation of sulfur dioxide at 193 nm. *Chem. Phys. Lett.* 148, 417–422 (1988).

Acknowledgements

The experimental research (A.G.S.) was supported by the Director, Office of Science, Office of Basic Energy Science, Division of Chemical Science, Geoscience and Bioscience of the US Department of Energy under contract no. DE-SC0017130 with additional support from the ARO under grant no. W911NF-17-1-0099. S.M. was supported by the NSF (CHE-1800171). The authors thank J. M. Bowman for comments on the manuscript and T. Sewell for helpful discussions.

Author contributions

H.L. and A.K. performed the experiments and analysed the data. H.L. and S.M. performed the theoretical calculations and analysed the results. A.G.S. conceived the experiments and guided the interpretation. H.L., S.M. and A.G.S. co-wrote the paper. All authors discussed the results and commented on the manuscript.

Competing interests

The authors declare no competing interests.

Additional information

 $\label{eq:supplementary} \textbf{Supplementary information} \ is \ available \ for \ this \ paper \ at \ https://doi.org/10.1038/s41557-018-0186-5.$

Reprints and permissions information is available at www.nature.com/reprints.

Correspondence and requests for materials should be addressed to A.G.S.

Publisher's note: Springer Nature remains neutral with regard to jurisdictional claims in published maps and institutional affiliations.

© The Author(s), under exclusive licence to Springer Nature Limited 2018